Supporting information

Fig. S1(a) shows the SEM image of a typical STO nanocrystal enclosed by low-indexed {001} facets and high-indexed {023} facets. Pt and PbO_2 nanoparticles were selectively deposited on the surface of STO by the photo-deposition method. It could be seen that Pt nanoparticles were deposited on {001} facets (Fig. S1(b)), while PbO_2 nanoparticles were deposited on {023} facets of STO (Fig. S1(c)). Therefore, during the photocatalytic process, the photoexcited electrons and holes in STO were transferred to the {001} and {023} facets, respectively, which were reported in Refs. [1, 2]. Thus, the photoreduction and photooxidation reactions occurred on the {001} and {023} facets of STO, respectively (Fig. S1(d)).

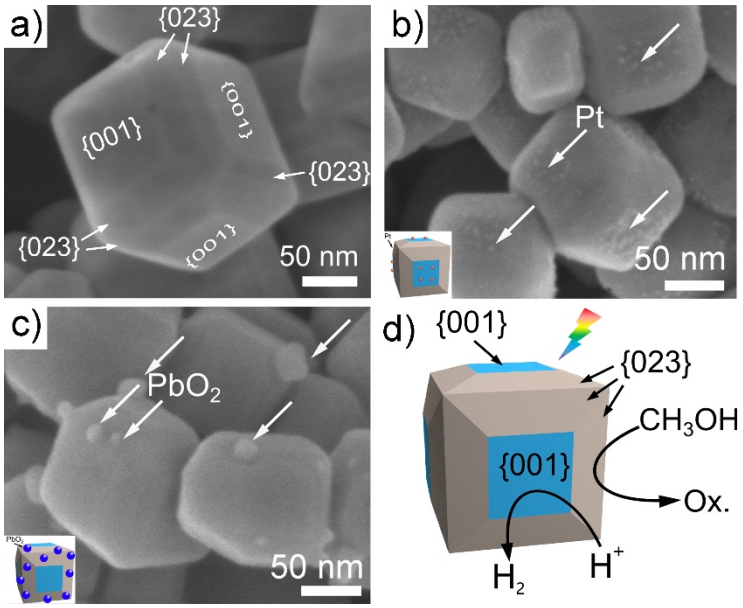

Fig. S1 SEM characterization of STO, STO-PD, STO-PbO_2 and diagram of photocatalytic mechanism for STO.

(a) a typical STO nanocrystal; (b) STO-PD; (c) STO-PbO_2; (d) photocatalytic redox reactions occurred on the {001} and {023} facets of STO. (The insets in (b) and (c) were the models of STO-PD, STO-PbO_2. White arrows in (b) and (c) indicate the representative Pt nanoparticles and PbO_2 nanoparticles, respectively.)

The XRD diffraction patterns of STO-PD and STO-CD were shown in Fig. S2(a). All the peaks for STO-PD and STO-CD were consistent, and no impurity peaks were observed. The peaks located at 2θ = 32.4°, 40.0°, 46.5°, 57.8°, 67.8°, and 77.2° in the XRD patterns of these two samples could be indexed to the (110), (111), (200), (211), (220) and (310) planes of $SrTiO_3$ (JCPDS No. 00-035-0734, space group: Pm-3m), confirming the cubic-phase perovskite structure of $SrTiO_3$ in these samples. No XRD peaks were observed due to the relatively low content of Pt in these samples. The sample STO-CD-CdS were synthesized by depositing CdS nanoshell on the surface of Pt nanoparticles of STO-CD *via* the photo-deposition method. It could be seen that the XRD peak positions of STO-CD-CdS were consistent with those of STO-PD and STO-CD, and no peaks of Pt for STO-CD-CdS were observed due to its low content (Fig. S2(a)). In the XRD pattern (Fig. S2(b)), a weak peak could be observed at 2θ = 26.5°, which could be indexed to the (111) plane of CdS, confirming the existence of CdS in STO-CD-CdS.

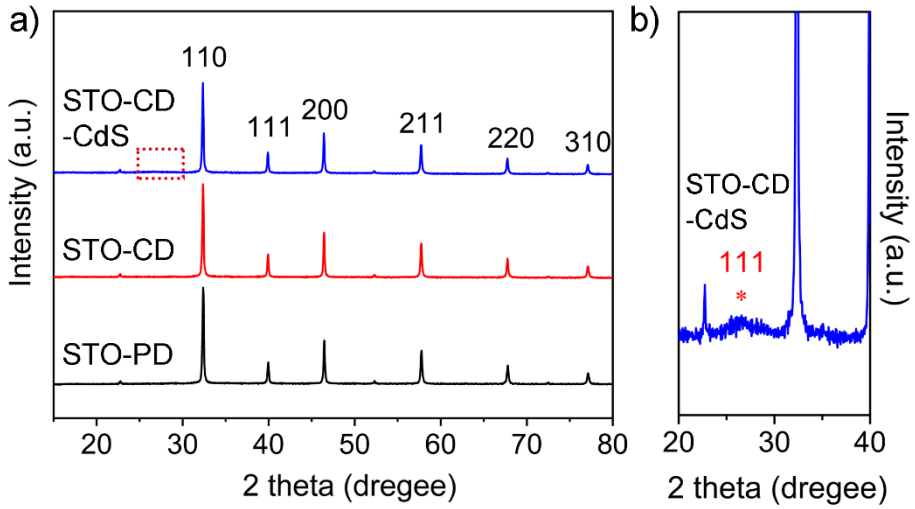

Fig. S2 Powder X-ray diffraction characterization of STO-PD, STO-CD and STO-CD-CdS.

a) XRD patterns of STO-PD, STO-CD and STO-CD-CdS; b) enlarged XRD patterns (2θ = 20 ^{o} −40^{o}) of STO-CD-CdS.

Figure S3 shows the SEM images of STO-CD. It could be seen that the islanded Pt nanoparticles were distributed on both {001} and {023} facets of STO-CD, as indicated

by the white arrows in Fig. S3, while for STO-PD, Pt nanoparticles were mainly deposited on the {001} facets of STO *via* the photo-deposition method (Fig. S1(b)).

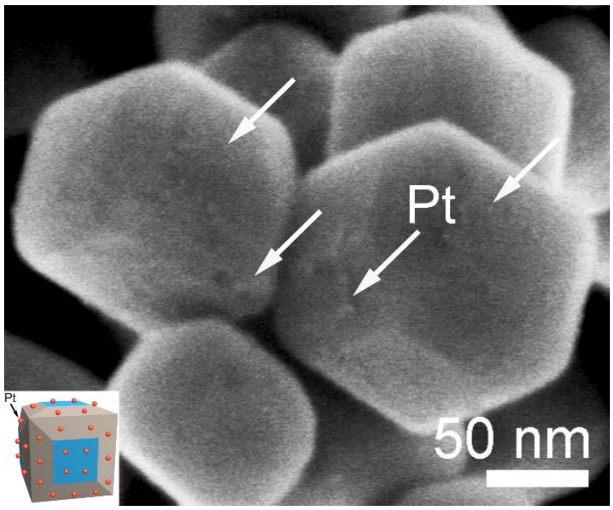

Fig. S3 SEM image of STO-CD.

X-ray photoelectron spectroscopy (XPS) characterization was conducted to investigate the chemical states of Pt nanoparticles on STO-PD and STO-CD, respectively, as shown in Fig. S4. The XPS peaks for the Pt nanoparticles deposited on both STO-PD and STO-CD were at 74.8 eV and 71.5 eV, respectively, confirming that the deposited Pt cocatalyst on the surface of STO-PD and STO-CD was in the form of Pt(0) [3, 4].

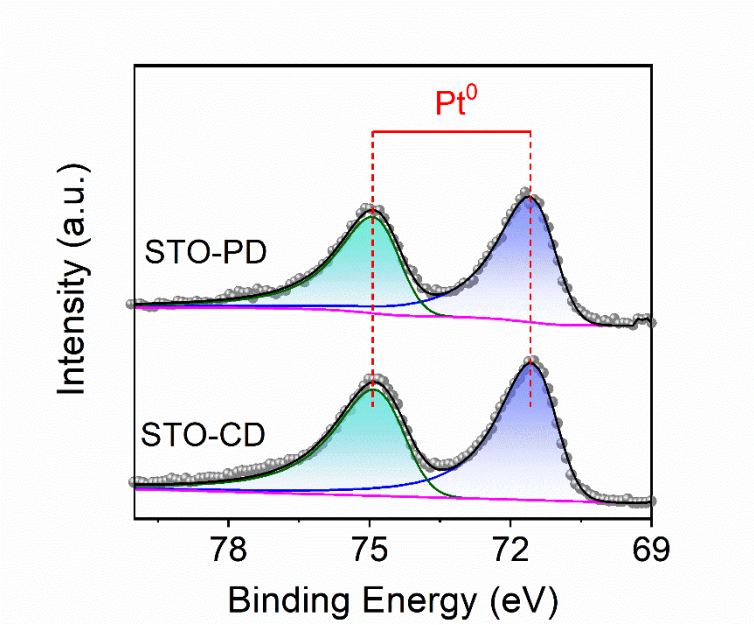

Fig. S4 XPS spectra of Pt 4f for STO-PD and STO-CD.

Figure S5(a) shows the TEM image of STO-PD nanocrystal viewed from [100] direction. It could be seen that some small particles were deposited only on the {001} facets of STO, and no nanoparticles were observed on the {023} facets. The HRTEM images in Figs. S5(b)–S5(d) were recorded from the rectangle I, II, and III regions, respectively. The interplanar space of the nanoparticles shown in Figs. S5(b)–S5(d) was measured to be 2.27 Å, corresponding to the (111) plane of Pt metal, and the size of Pt nanoparticles was less than 5 nm, which was similar to that of Pt nanoparticles on STO-CD.

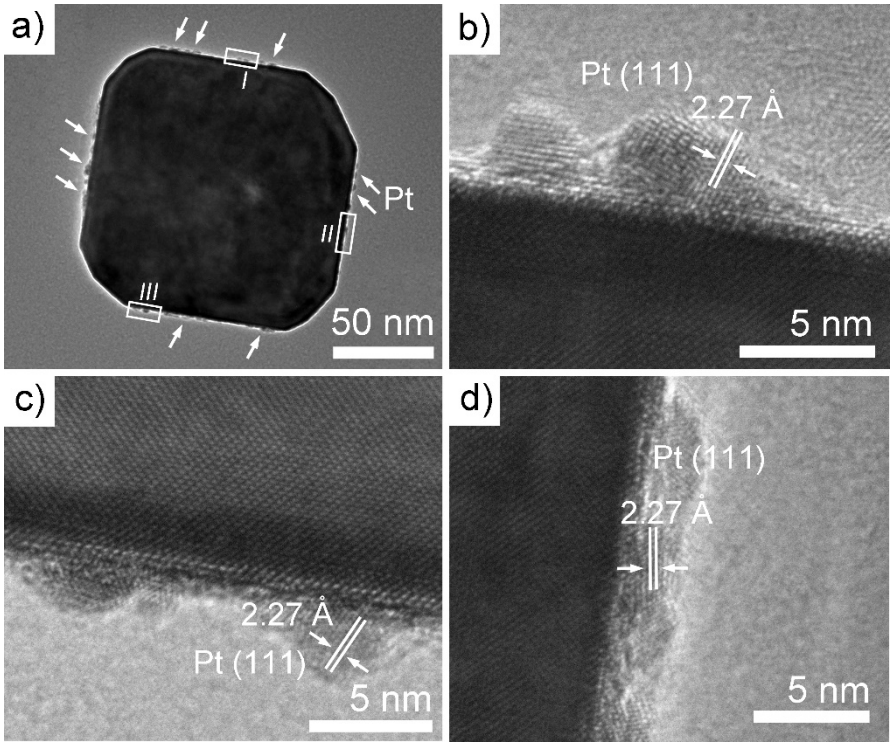

Fig. S5 TEM characterization of STO-PD.

(a) TEM image of a typical STO-PD nanocrystal viewed from [100] direction; (b, d) HRTEM images recorded from the rectangle b) I, c) II, d) III regions, respectively.

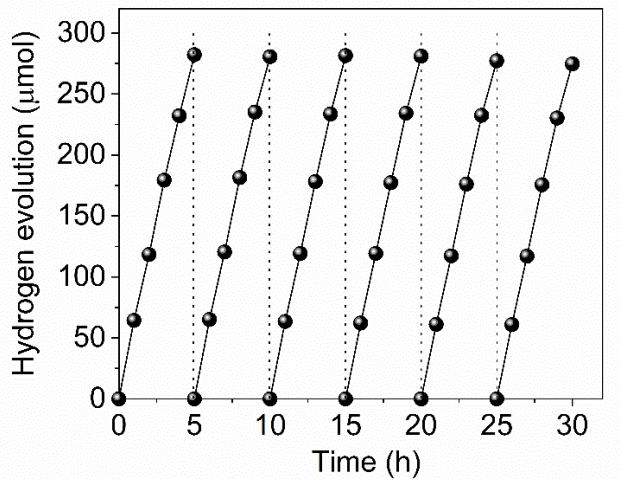

Fig. S6 cycles experiments of photocatalytic H_2 evolution over STO-CD.

Figure S7 shows the UV-vis absorption spectra of STO-CD and STO-CD-CdS. Compared with STO-CD, the STO-CD-CdS exhibited an obvious absorption band in the range of 400−550 nm, which should be ascribed to the CdS nanoshell on the surface of Pt nanoparticles deposited on both {023} and {001} facets of STO.

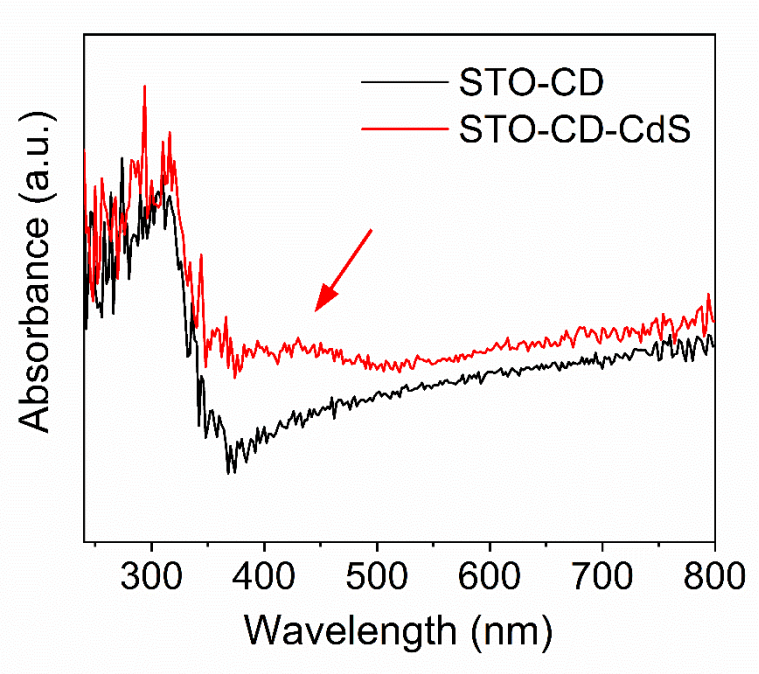

Fig. S7 Uv-vis absorption spectra of STO-CD and STO-CD-CdS.

Figure S8 shows the XPS spectra of Cd 3d and S 2p of STO-CD-CdS. The Cd 3d XPS spectrum (Fig. S8(a)) showed two peaks at 411.8 and 405.0 eV, respectively, which corresponded to Cd^{2+} species [5]. The XPS peaks at 162.5 and 161.2 eV in Fig. S8(b)

could be assigned to S^{2-} sulfur species [6]. Thus, the results of Cd 3d and S 2p XPS spectra further confirmed the existence of CdS in STO-CD-CdS.

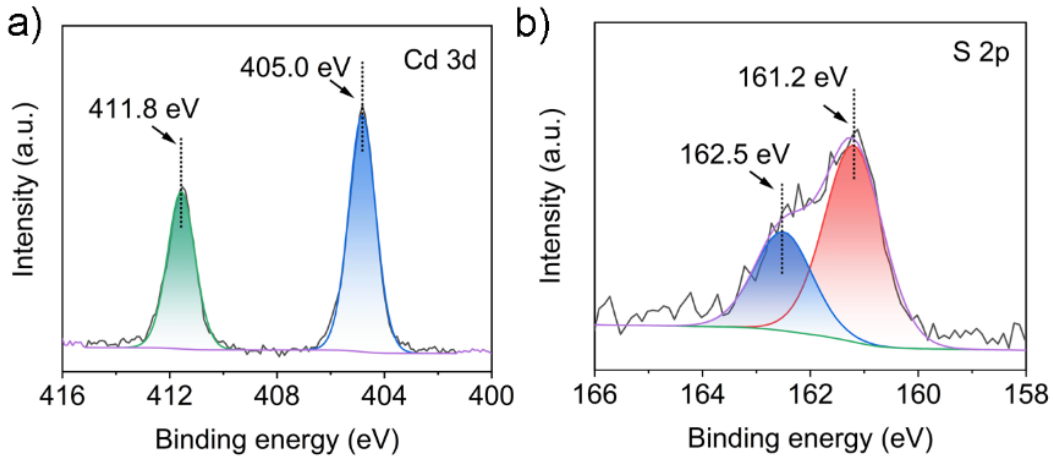

Fig. S8 XPS spectra of STO-CD-CdS.

(a) Cd 3d; (b) S 2p.

References

[1] Wang B, Shen S, Guo L. $SrTiO_3$ single crystals enclosed with high-indexed {023} facets and {001} facets for photocatalytic hydrogen and oxygen evolution. Appl. Catal. B, 2015, 166−167: 320−326

[2] Wang B, Shen S, Guo L., Surface reconstruction of facet-functionalized $SrTiO_3$ nanocrystals for photocatalytic hydrogen evolution. ChemCatChem, 2016, 8: 798−804

[3] Hosseini F, Safaei E, Mohebbi S. Modified WO_3 nanorod with Pt nanoparticle as retrievable materials in catalytic and photocatalytic aerobic oxidation of alcohols. J. Nanopart. Res., 2017, 19: 240

[4] Chen Y C,, Sun Y M,, Gan J Y. Improved fatigue properties of lead zirconate titanate films made on oxygen-implanted platinum electrodes. Thin Solid Films, 2004, 460: 25−29

[5] Deng F, Lu X, Luo Y,et al.Novel visible-light-driven direct Z-scheme CdS/$CuInS_2$

nanoplates for excellent photocatalytic degradation performance and highly-efficient Cr(VI) reduction. Chem. Eng. J., 2019, 361: 1451−1461

[6] Kartio I J, Basilio C I, Yoon R H. An XPS study of sphalerite activation by copper. Langmuir, 1998, 14: 5274−5278